Molecular Therapy
Original Article

Effective and Accurate Gene Silencing by a Recombinant AAV-Compatible MicroRNA Scaffold

Jun Xie,[1,2,3,4] Phillip W.L. Tai,[1,3,4] Alexander Brown,[1,3,4] Shoufang Gong,[1,3,4] Sha Zhu,[1,3,4] Yi Wang,[1,3,4,5] Chengjian Li,[6] Cansu Colpan,[7] Qin Su,[1,2,3] Ran He,[1,2,3] Hong Ma,[1,2,3] Jia Li,[1,3,4] Hanqing Ye,[1,3,4] Jihye Ko,[1,2,3] Phillip D. Zamore,[7] and Guangping Gao[1,2,3,4]

[1]Horae Gene Therapy Center, University of Massachusetts Medical School, Worcester, MA, USA; [2]Viral Vector Core, University of Massachusetts Medical School, Worcester, MA, USA; [3]Li Weibo Institute for Rare Diseases Research, University of Massachusetts Medical School, Worcester, MA, USA; [4]Department of Microbiology and Physiological Systems, University of Massachusetts Medical School, Worcester, MA, USA; [5]Research Unit of Infection and Immunity, Department of Pathophysiology, West China College of Basic and Forensic Medicine, Sichuan University, Chengdu, Sichuan, People's Republic of China; [6]Fornax Biotech, Worcester, MA, USA; [7]RNA Therapeutics Institute and Howard Hughes Medical Institute, University of Massachusetts Medical School, Worcester, MA, USA

Short hairpin RNAs that are delivered by recombinant adeno-associated virus (rAAV) have the potential to elicit long-term RNAi therapy for human disease. However, the discovery that short hairpin sequences can cause truncation of the rAAV genome calls into question the efficiency and gene-silencing specificity of this strategy in humans. Here, we report that embedding the guide strand of a small silencing RNA into an artificial microRNA (miRNA) scaffold derived from mouse *miRNA-33* ensures rAAV genomic integrity and reduces off-targeting by 10-fold, while maintaining effective *in vivo* target gene repression in mice.

INTRODUCTION

The RNA interference (RNAi) pathway uses small RNA guides to direct Argonaute (AGO) proteins to slice an mRNA target in two, thereby silencing its expression.[1] Exogenous small double-stranded RNAs can co-opt this process by mimicking endogenous triggers, enabling gene knockdown for research or therapy.[2] Unlike chemically modified small interfering RNAs, short hairpin RNAs (shRNAs) can be delivered by recombinant adeno-associated viruses (rAAVs), viral vectors that can efficiently transfer foreign genes into many tissues and provide long-term transgene expression with no known pathogenic consequences.[3] However, high levels of AAV-delivered shRNAs can perturb the RNAi machinery, leading to cellular toxicity.[4,5] Reducing the amount of shRNA by lowering vector doses, selecting less efficient AAV serotypes, or using weaker RNA polymerase (Pol) II promoters, instead of a strong and constitutive *H1* or *U6* Pol III promoters, can prevent toxicity.[5,6] Alternatively, embedding the antisense RNA in endogenous microRNA (miRNA) scaffolds may improve small RNA processing, express multiple silencing RNAs against one or multiple target genes, and alleviate RNAi toxicity.[5,7–10] However, each of these strategies has thus far compromised RNAi potency.[5,11]

Off-target activity poses a second hurdle for RNAi applications. Off-target gene silencing can complicate data interpretation in functional studies and raises safety concerns for RNAi-based therapies.[12] Undesirable incorporation of the passenger strand into AGO and fortuitous complementarity of the guide strand seed sequence (positions g2–g8) with non-target mRNAs can trigger miRNA-like repression of off-target genes. Because the seed sequence is determined by the position of the 5′ end of the small RNA, heterogeneity at the 5′ end increases the potential for miRNA-like off-target activity and is a common problem with transcribed shRNAs.[13–15] Identifying designs that promote accurate processing of shRNAs remains a crucial step for rAAV-delivered RNAi.

Beyond these shRNA-specific challenges, our previous work has shown that shRNA-encoded sequences redirect rAAV viral genome replication, generating truncated rAAV genomes lacking an intact shRNA cassette.[16] This discovery highlights the importance of developing AAV-compatible gene-silencing vectors that retain high efficacy, confer minimal off-targeting, and yield a high proportion of intact viral genomes during vector production.

RESULTS

Thermodynamic Stability of shRNA-Encoding Sequences Influences AAV Genome Integrity

We previously reported that shRNA cassettes in rAAV genomes can hinder and redirect rAAV genome replication, leading to

Received 25 April 2019; accepted 21 November 2019;
https://doi.org/10.1016/j.ymthe.2019.11.018.

Correspondence: Jun Xie, Horae Gene Therapy Center, University of Massachusetts Medical School, Worcester, MA, USA.
E-mail: jun.xie@umassmed.edu
Correspondence: Phillip D. Zamore, RNA Therapeutics Institute and Howard Hughes Medical Institute, University of Massachusetts Medical School, Worcester, MA, USA.
E-mail: phillip.zamore@umassmed.edu
Correspondence: Guangping Gao, Horae Gene Therapy Center, University of Massachusetts Medical School, Worcester, MA, USA.
E-mail: guangping.gao@umassmed.edu

heterogeneous populations comprising a mixture of full-length genomes and truncated vector species that lack the capacity to silence mRNAs. Stable base pairing between sequences that encode the passenger and guide strands can cause truncation events.[16] We hypothesized that introducing mismatches into the shRNA stem may improve rAAV genome integrity. To test this idea, we introduced up to four dinucleotide bulges at different positions in the passenger strand, while keeping the guide strand of an shRNA against mouse apolipoprotein B transcripts (*shApob*) unchanged (Figure 1A). The *shApob* cassettes that carry bulges were incorporated into the self-complementary (sc)AAV-*CB-Egfp* construct, within the intron residing between the *Egfp* coding sequence and the cytomegalovirus (*CMV*) enhancer/chicken β-actin (*CB*) promoter. We co-transfected these scAAV-*shApob* plasmids with pAdeno-helper and *pRep2/Cap9* plasmids into HEK293 cells and analyzed low-molecular-weight DNAs. Southern blot analysis revealed that overall, *shApob* cassettes with bulges generated fewer truncated genomes than cassettes without bulges (Figure 1B). *shApob* cassettes with lower thermodynamic stabilities yielded fewer truncated genomes (Figure 1C). To quantify the gene-silencing efficiencies of *shApob* cassettes that carry bulges, we co-transfected *shApob* constructs with a pmiCHECK-*Apob* sensor plasmid containing an *Apob*-coding sequence placed in the 3′ UTR of the *β-Gal* reporter gene (Figures 1D and 1E). Lowering the thermodynamic stability of the shRNA stem improved rAAV genome integrity (Figures 1B and 1C), but at the cost of reduced RNAi efficacy (Figures 1D and 1E). The large abundance of unprocessed shRNA precursors and less antisense small RNA likely explain the low RNAi efficacies observed from bulged-*shApob* cassettes (Figure S1).

The miR-33 Scaffold Improves rAAV Genome Integrity

We tested whether natural pre-miRNA scaffolds could improve rAAV genome integrity without compromising efficacy. Unlike artificial shRNAs, endogenous miRNAs precursors (pre-miRNAs) typically bear mismatches within their stems. First, we designed and packaged capsids with rAAV constructs harboring DNA sequences derived from 15 different mouse primary miRNAs (pri-miRNAs), transcripts that undergo sequential processing into pre-miRNAs and then into miRNAs. Agarose gel analysis of viral DNA showed that the frequency of genome truncation varied among the tested pri-miRNAs (Figure 2A). We next used pri-miRNAs as scaffolds to house the *Apob* antisense sequence. For each artificial miRNA scaffold (shRNA^{miRNA}), the original miRNA guide was replaced with the *shApob* guide strand; bulges were incorporated into the passenger strands to mimic the native structure of the endogenous pre-miRNA. Each construct incorporated both the pre-miRNA loop and ∼100 nt of flanking sequence derived from the corresponding mouse pri-miRNAs. Figure 2B illustrates the *shApob* guide that is embedded within the *mmu*-pri-miR-33 scaffold. We measured RNAi potency for conventional shApob- and shApob^{miRNA}-expressing plasmids in HEK293 cells. Transcription of shRNA$^{miR\text{-}33}$ and shRNA$^{miR\text{-}155}$ was driven by the RNA Pol II *CB* promoter. These activities triggered reporter silencing comparable with that produced by conventional shRNA constructs transcribed by RNA Pol III from the *H1* promoter (Figure 2C). We packaged each of the shRNA^{miRNA}-expressing constructs into AAV and examined genome integrity of the purified vectors. The shApob vector encapsidated 20% full-length genomes, whereas miR-33 (shApob$^{miR\text{-}33}$) and miR-155 (shApob$^{miR\text{-}155}$) scaffolds packaged 75% and 40% intact genomes, respectively (Figure 2D). AAV vectors harboring shRNAs against the firefly luciferase reporter gene (*Fluc*), mouse ectonucleotide pyrophosphatase/phosphodiesterase 1 (*PC*-1), or human cytosolic Cu/Zn superoxide dismutase 1 (*SOD-1*) exhibited 12%, 25%, and 36% full-length genomes, respectively. In contrast, their counterparts using the miR-33 scaffold increased the percentage of full-length genomes to 68%, 72%, and 63%, respectively (Figure 2E). By introducing bulges into the short hairpin DNA, the miR-33 scaffold improved rAAV genome integrity from 28% ± 10% to 69% ± 4%. Faint bands that were attributed to small truncated genomes were still observed (Figures 2D and 2E) and are likely caused by the palindromic sequences residing in other regions of the vector as previously reported.[16]

miR-33 Scaffolds Achieve Effective Gene Silencing in Cultured Cells and Mice

Next, we compared the gene-silencing efficacies of shRNAs and their counterpart *miR-33* scaffolds in HEK293 cells and mice. Knockdown efficacy of the shRNA$^{miR\text{-}33}$ constructs targeting *Apob* (Figure 2C), *Fluc*, *PC-1*, and *SOD-1* in HEK293 cells was as potent as the counterpart shRNAs driven by the strong *U6* or *H1* Pol III promoter (Figure 3A).

Features that enable efficient processing of pri-miRNAs have been described previously.[17,18] Incorporating some of these motifs into artificial *miR-30* and *miR-155* scaffolds has been shown to confer increased RNAi potency.[9,19] The *mmu-pri-miR-33* transcript contains nearly all features of an optimal miRNA,[17,18] including a 35-bp stem, a UG motif at the 5′ end of the pre-miRNA, a mismatched GHG motif in the stem, a UGUG motif in the loop, and a CNNC motif downstream of the pre-miRNA 3′ end (Figure S2A). We converted the sub-optimal nucleotides in *mmu*-pri-miR-33 into the exact motifs of *de novo* designed miRNA[18] to generate two additional scaffolds, miR-33-m and miR-33-p (Figure S2A, bottom). *miR-33-m* possesses a bulged-stem similar to endogenous *miR-33*, whereas *miR-33-p* carries a perfectly complementary stem. Dose-response analyses showed that the respective vector activities of the modified *miR-33* scaffolds were more efficient than the non-optimized *shApob*$^{miR\text{-}33}$ vector (Figure S2B, top), comparable with the non-optimized *shPC-1*$^{miR\text{-}33}$ vector (Figure S2B, middle), and less efficient than the non-optimized *shSOD1*^{miR33} vector (Figure S2B, bottom). Overall, the introduction of optimal miRNA motifs failed to consistently enhance the potency of the *miR-33* scaffold.

We packaged constructs harboring shRNA$^{miR\text{-}33}$ within the intron or shRNA next to the mutant terminal repeat or within the intron into AAV capsids (Figure S3A). We positioned the shRNA next to the mutant terminal repeat to decrease the proportion of truncated genomes[16] (Figures S3B–S3D, *shRNA-mp* in lane 3). The vectors were intravenously injected into adult mice. After 3 weeks, we used

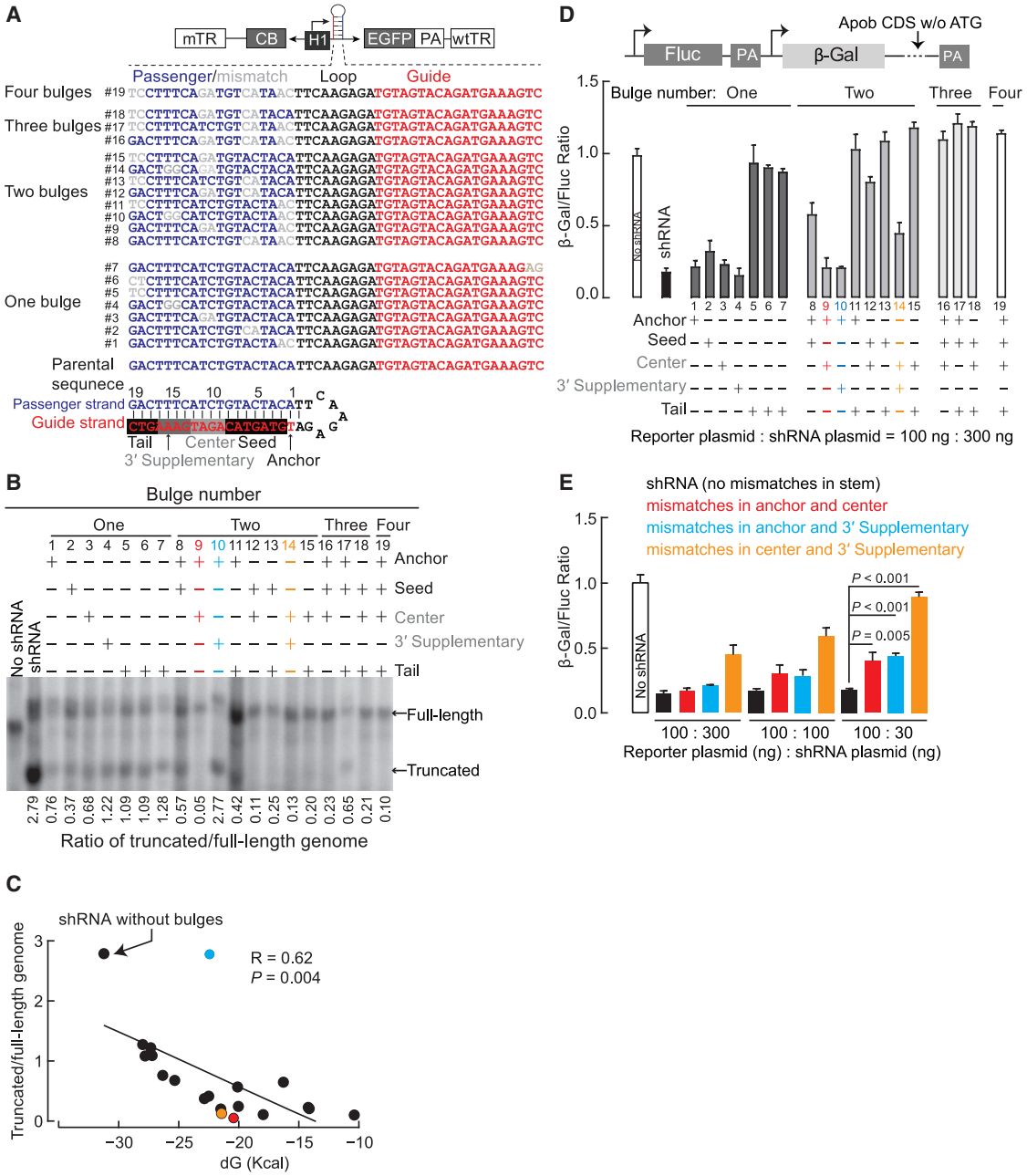

Figure 1. Thermodynamic Stability of the shRNA Stem Influences rAAV Genome Homogeneity

(A) Diagram of the self-complementary (sc)AAV construct carrying shApob sequences within the intronic region between the *CMV* enhancer/chicken β-actin (*CB*) promoter and the *Egfp* transgene. Nucleotide mismatches are in gray. (B) Southern blot analysis of low-molecular-weight DNA extracted from HEK293 cells transfected with the scAAV-*shApob* plasmid, p*Rep2/Cap9* plasmid, and pAdeno-helper plasmid using ^{32}P-labeled EGFP probe. (C) Correlation between the thermodynamic stabilities of short hairpin DNA and their ratios of truncated AAV genome to full-length genomes. The ΔG values were calculated with RNAfold. (D) Ratios of β-galactosidase (*β-Gal*) and Firefly luciferase (*Fluc*) in HEK293 cells co-transfected with *shApob* constructs and a sensor plasmid carrying the *Apob* coding sequence in the 3′ UTR of *β-Gal*. After 48 h, *Fluc* and *β-Gal* levels were measured, and the ratio between *β-Gal* and *Fluc* was calculated to reflect the gene-silencing efficacies. (E) Relative β-galactosidase activity in HEK293 transfected with sensor plasmid and RNAi plasmids at different ratios. Colored scheme in (C) (dots) correlates with the construct types indicated in the legend (E). The amount of sensor plasmid and *shApob* plasmid for transfection is indicated. mTR, mutant TR; TR, terminal repeat. Values are mean ± SD.

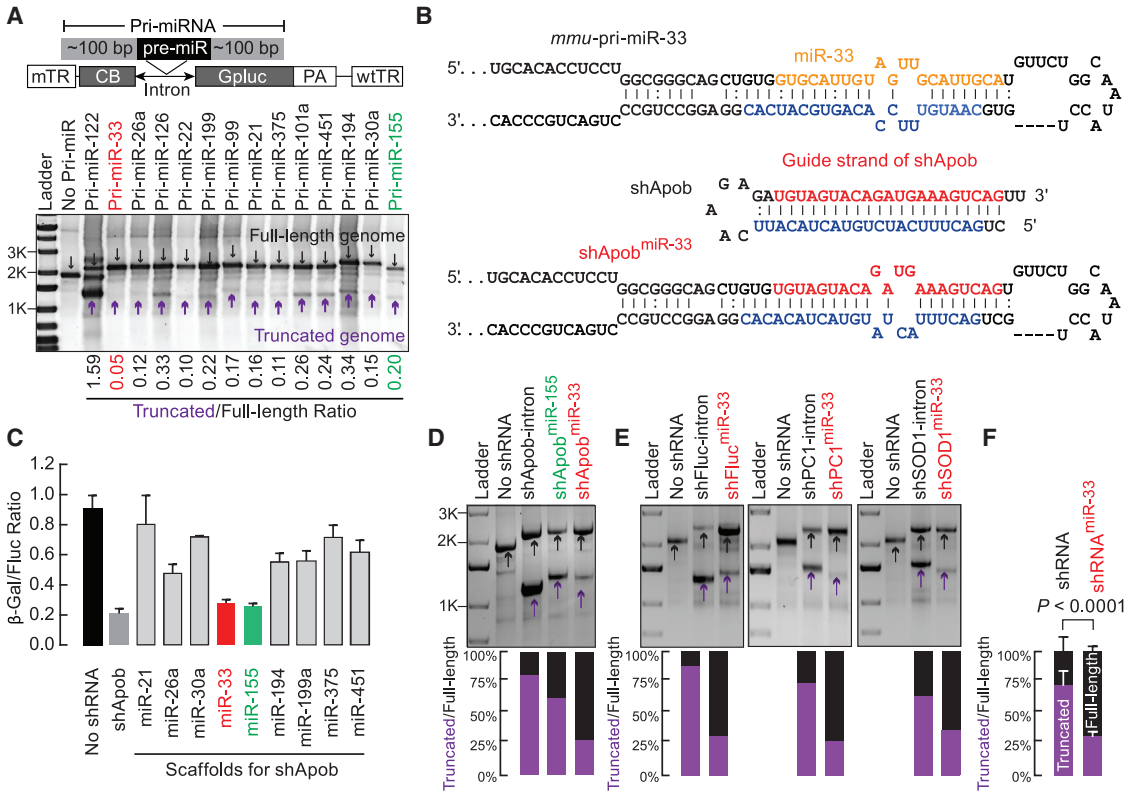

Figure 2. The *miR-33* Scaffold Reduces the Prevalence of Vector Genome Truncations Caused by Short DNA Hairpins

(A) Top: viral genome schematic of scAAV8 vectors carrying pri-miRNA fragments that contain pre-miRNA and ~100-bp flanking sequences at each end. Bottom: a representative 1% agarose gel of viral genomes isolated from packaged vectors. (B) Design of artificial miRNA constructs using the *miR-33* scaffold. An Excel macro was developed to embed the shRNA into the *miR-33* scaffold (Data S1). (C) Comparisons of gene-silencing efficiencies between miRNA scaffolds and conventional *shApob* in HEK293 cells. Plasmids expressing RNA inhibitors were co-transfected with a *β-Gal* sensor plasmid into HEK293 cells at 200 and 60 ng/well, respectively. Relative reduction in β-Gal activity reflects knockdown efficacy. (D) Agarose gel analysis of genomic DNA from purified vectors that carry no shRNA, *shApob*, artificial *miR-155*, or *miR-33* against *Apob* (*shApob*$^{miR\text{-}155}$ or *shApob*$^{miR\text{-}33}$). (E) Agarose gel analyses of viral DNA extracted from purified vectors that harbor shRNA or shRNA$^{miR\text{-}33}$ against *Fluc*, *PC-1*, or *SOD-1*. (F) Summary of the ratios between truncated and full-length genomes from vectors harboring shRNA or *shApob*$^{miR\text{-}33}$ against *Apob1*, *Fluc*, *PC-1*, or *SOD-1*. Fisher's exact test was used. (D–F) The ratios of truncated and full-length genomes were calculated using band intensities and normalized to their molecular sizes. Purple arrows indicate truncated genomes. Black arrows indicate full-length genomes. Values are mean ± SD.

live bioluminescence imaging (Figure S4) and quantified luciferase activities in liver extracts (Figure 3B) to measure *Fluc* expression in mice previously co-administered a rAAV9-*Fluc* reporter vector and a gene-silencing vector. For mice receiving gene-silencing vectors against *PC*-1 or *Apob*-1, liver mRNA levels were assessed by quantitative reverse transcription-PCR (qRT-PCR; Figures 3C and 3D). Compared with AAV-shRNA vectors, shRNA$^{miR\text{-}33}$ vectors achieved comparable gene silencing of *fluc* and *pc-1* mRNA, and a greater reduction of *apob* mRNA in mice. Thus, in cultured cells and mice, the *miR-33* scaffold effectively mediates gene silencing that is comparable with conventional Pol III promoter-driven shRNAs.

Small RNAs Transcribed from *miR-33* Scaffolds Are Efficiently Processed in Cultured Cells

We next evaluated RNA processing in HEK293 cells transfected with shRNA or *shRNA*$^{miR\text{-}33}$ plasmids by northern blot analysis. For the *shApob* construct, we detected two isoforms of guide strand and one passenger strand isoform. In contrast, we detected one guide strand isoform and an absence of a passenger strand isoform for the *shApob*$^{miR\text{-}33}$ construct (Figure 4A). For the *shSOD1* construct, we detected one isoform of guide strand and two isoforms of passenger strand, whereas for the *shSOD1*$^{miR\text{-}33}$ construct, only the mature guide and passenger strand were detected (Figure S5A). For the *shPC-1* construct, there were two isoforms for both strands, whereas the *shPC-1*$^{miR\text{-}33}$ construct produced one guide strand isoform and one passenger strand isoform (Figure S5B). We concluded that shRNA$^{miR\text{-}33}$ plasmids generate less unprocessed guide and passenger strand isoforms compared with shRNA plasmids. Furthermore, the *miR-33* scaffold increased the ratio of mature guide to passenger strand in two of three scaffolds tested (Figure 4B). The miR-33 scaffold was especially useful for improving poorly processed shRNAs, as in the case of the low guide/passenger strand ratio for *shSOD1* (Figure 4B; Figure S5A). In summary, transcribed RNAs from *miR-33* scaffolds were accurately and efficiently processed, yielding little unprocessed precursor, high

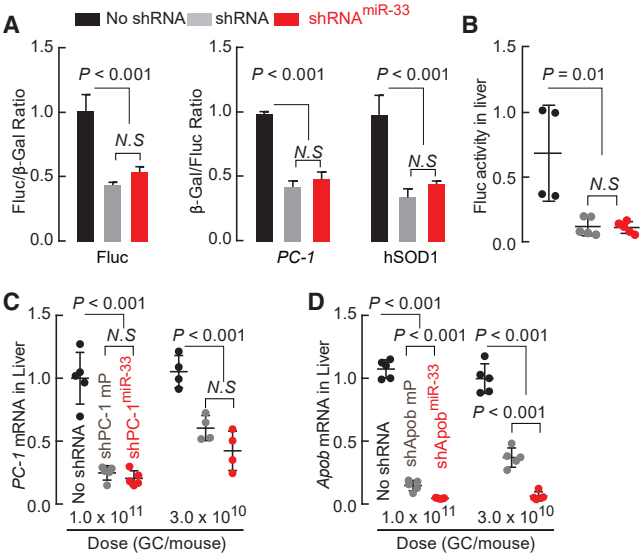

Figure 3. *miR-33*-Scaffolded shRNAs Promote Efficient Gene Silencing in Cultured Cells and Mice

(A) Relative reporter activity in HEK293 cells transfected with *Fluc*, *PC-1*, and *SOD1* gene-silencing constructs and their sensor plasmids. (B) Firefly luciferase activities detected in treated mouse liver extracts. Mice were co-administrated with rAAV9-*Fluc* reporter vector at 1.0×10^{11} GCs/mouse and the gene-silencing vectors rAAV9-*shFluc* (n = 5), *shFluc*$^{miR\text{-}33}$ (n = 5), or no shRNA (n = 4) at 5.0×10^{11} GCs/mouse. After 3 weeks, mice were sacrificed to assess firefly luciferase activity. (C) *pc*-1 mRNA levels in the livers of mice treated with rAAV9-*shPC-1* or rAAV9-*shPC-1*$^{miR\text{-}33}$. Five mice in the 1.0×10^{11} GCs/mouse group and four mice in the 3.0×10^{10} GCs/mouse group. (D) *apob* mRNA levels in the livers of mice (n = 5 in each group) treated with rAAV9-shApob or rAAV9-*shApob*$^{miR\text{-}33}$. rAAVs at the indicated doses were injected into adult C57BL/6 mice by tail vein. After 3 weeks, mice were sacrificed for *PC-1* and *Apob* gene expression analysis using qRT-PCR. *shFluc* is driven by the *U6* promoter. *shApob*, *shPC-1*, and *shSOD-1* are driven by the *H1* promoter. Values are mean ± SD. GC, genome copy.

guide-to-passenger strand ratios, and levels of mature guide strand comparable with conventional Pol III promoter-driven shRNAs.

The miR-33 Scaffold Generates More Accurate Gene Silencing in Mice

To assess RNAi accuracy conferred by the *miR-33*-scaffolded cassettes, we sequenced exogenously expressed shRNAs, endogenous miRNAs, and mRNAs of mouse livers treated with AAV-*shPC-1* or AAV-*shPC-1*$^{miR\text{-}33}$ vectors (Figures 5A–5C).

Both the conventional shRNA and the shRNA$^{miR\text{-}33}$ scaffold promoted efficient loading of the guide strand into AGO: passenger strands were <0.2% of small RNAs generated from mice receiving *shPC-1* (guide strand, [85 ± 6] × 10^3 ppm; passenger strand, 91 ± 8 ppm; guide/passenger strand ratio, [953 ± 34]-fold) or *shPC-1*$^{miR\text{-}33}$ (guide strand, [83 ± 16] × 10^3 ppm; passenger strand, 48 ± 12 ppm; guide/passenger strand ratio, [1,878 ± 402]-fold). However, the 5′ ends of the *shPC-1*-derived guide strands were highly heterogeneous, and the majority of 5′ ends were 3′-shifted by one to four nucleotides for AAV-*shPC-1*, producing four different seeds. Notably, 99.50% ± 0.03% of the AAV-*shPC-1* guides differed from the desired sequence. In contrast, *shPC-1*$^{miR\text{-}33}$ generated just 0.3% ± 0.2% incorrect 5′ ends among >2.2 ± 0.4 million guide strand reads (Figure 5A). Thus, *shPC-1*$^{miR\text{-}33}$ effectively produces only a single guide sequence.

The conventionally designed shPC-1, but not the *shPC-1*$^{miR\text{-}33}$ vector, also perturbed endogenous miRNA levels: small-RNA profiling of mouse livers treated with AAV-shPC-1 revealed 13 significantly dysregulated miRNAs (>2-fold change and false discovery rate [FDR] < 0.05), whereas no significant changes in miRNA expression were observed in mice receiving AAV-*shPC-1*$^{miR\text{-}33}$ (Figure 5B).

Similarly, the conventional *shPC-1*, but not the *shPC-1*$^{miR\text{-}33}$ vector, perturbed mRNA expression. Compared with a control AAV vector lacking a shRNA cassette, the AAV-*shPC-1* vector altered expression of 2,541 genes (FDR < 0.05; 1,215 decreased and 1,326 increased). In contrast, injection of AAV-*shPC-1*$^{miR\text{-}33}$ decreased expression of just 93 genes and increased expression of 124 genes. Not including *pc-1*, the *shPC-1* sequence contains seed matches to many mRNAs whose steady-state abundance decreased: 535 contained a guide+1 seed match, 657 contained a guide+2 seed match, 770 contained a guide+3 seed match, and 980 contained a guide+4 seed match (Figure S6; Table S2). In contrast, 41 decreased mRNAs harbored a match to the *shPC-1*$^{miR\text{-}33}$ seed sequence (Figure S6; Table S3). Among these dysregulated genes, 9 decreased and 12 increased genes were also found in patients with a *PC-1* loss-of-function mutation (Table S4).[20] Finally, *shPC-1*, but not *shPC-1*$^{miR\text{-}33}$, changed the abundance of mRNAs encoding RNAi pathway proteins (AGO1, AGO2, AGO3, DICER1, DROSHA, and PACT), suggesting that AAV-shRNA vectors not only perturb global liver gene expression, but also disrupt the miRNA pathway itself (Figures 5C and 5D).

DISCUSSION

Efficient and specific gene silencing are critical challenges for RNAi therapeutics.[21] shRNA-encoded sequences can redirect rAAV viral genome replication, generating truncated rAAV genomes lacking an intact shRNA cassette to produce silencing RNA.[16] Here, we showed that Pol II *CB* promoter-driven *miR-33*-scaffolded shRNAs can confer gene knockdown in cultured cells and mice at levels that are comparable with conventional Pol III promoter-driven shRNA constructs, while achieving the accuracy that is lacking with conventional shRNAs. Importantly, the *miR-33* scaffold exhibits reduced frequency of truncated viral vector genomes.

Consistent with the previous observations on Pol III promoter-driven shRNA,[13–15] the 5′ ends of guide strands are highly heterogenous due to imprecise cutting by Dicer. The accuracy of Dicer processing can be greatly improved by optimizing the loop position of shRNAs.[15] By contrast, the *miR-33* scaffold generates a unique seed sequence. Other miRNA scaffolds also showed accurate processing of the guide strands.[7,13,14] Similar to endogenous miRNAs, which have unique seed sequences, the artificial miRNAs are processed by Drosha and

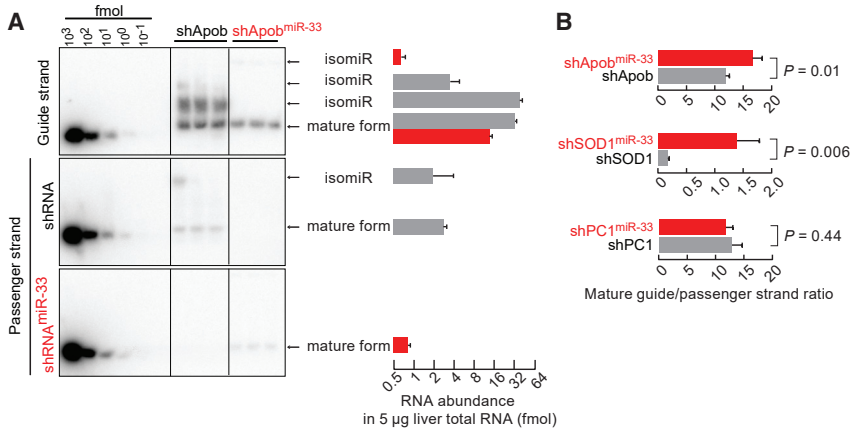

Figure 4. Small RNA Processing in HEK293 Cells

(A) Northern blot analysis of small RNAs in HEK293 cells transfected with *shApob* or *shApob*$^{miR\text{-}33}$ plasmids. Total RNA was extracted from the HEK293 cells 48 h after transfection. Five micrograms of total RNA was used for northern blot analysis. Synthetic oligonucleotides at indicated amounts were used as reference for quantification. shRNA and shRNA$^{miR\text{-}33}$ plasmids transcribe the same guide strand (top), but different passenger strands (middle and bottom). The transcribed RNAs from *shApob* and *shApob*$^{miR\text{-}33}$ are in gray and red, respectively. (B) Ratios of mature small RNA guide strand and passenger strand detected from *shApob*, *shSOD-1*, *shPC-1*, and their counterpart *miR-33* scaffolds. Values are mean ± SD.

Dicer by mimicking the endogenous miRNA, ensuring accurate processing at the 5′ ends of mature siRNAs.

Artificial miRNAs have been used for RNAi, but their efficacies have generally been less than RNA Pol III-transcribed shRNAs.[5,11] *U6* and *H1* Pol III promoter-driven *SOD-1*$^{miR\text{-}155}$ cassettes were shown to be more efficient at gene knockdown than cassettes with *SOD-1*$^{miR\text{-}155}$ that are driven by a Pol II *CB* promoter. However, they also led to elevated liver transaminases in macaques.[22] The *miR-33* scaffold efficiently and accurately reduces target expression, making it a promising platform for AAV-mediated RNAi gene therapy for fatal neurodegenerative diseases such as Huntington's disease and amyotrophic lateral sclerosis.

Previous studies have proposed optimizing the shRNA design to alleviate off-target effects caused by incorporation of passenger strands into AGOs.[23,24] Although several miRNA scaffolds have been reported to yield effective and safe gene silencing (e.g., *miR-30*,[15] *miR-155*,[7,15] and *miR-223*[13]), the *miR-33* scaffold accurately processes the guide strand and yields the highest ratio of guide to passenger strand, eliminating the need for more complex strategies such as co-expressing RNA decoys.[25]

shRNA$^{miR\text{-}33}$, with its less thermostable stem, produced fewer truncated genomes compared with other miRNA scaffolds (Figures 2A and 2D). Moreover, the reduction in thermodynamic stability enhances the rate-limiting step of unwinding the siRNA duplex for noncleaving mammalian AGO1, AGO3, and AGO4 proteins.[26,27] Screening or optimizing gene-silencing scaffolds with low thermostabilities marks a new direction for the development of high-efficiency, rAAV-compatible gene-silencing platforms. Although the *miR-33* scaffold's stem mismatches significantly reduce the proportion of truncated genomes, its stem-loop structure still causes some truncation events (Figures 2D and 2E). More comprehensive screening of endogenous pri-miRNA scaffolds along with optimized guide sequences may further reduce genome heterogeneity and increase RNAi potency. Optimization of current rAAV vector production systems to include modification of factors that can facilitate error-free DNA replication through palindromic sequences may improve rAAV homogeneity for clinical applications. Because of their small sizes, most gene-silencing expression cassettes are engineered into scAAV vectors, which can bypass the rate-limiting step of second-strand synthesis for robust transduction. In the context of single-stranded AAV genome, the high thermodynamic stability of shRNA-encoding sequences also leads to truncated vector genomes,[16] which may further compromise the *in vivo* genome stability and functionality. The incorporation of guide sequences into the *miR-33* scaffold can be easily accomplished using a simple Excel Macro we have developed (Data S1). The *miR-33* scaffold also allows for transcription by RNA Pol II, creating safe inducible or tissue- or cell-type-specific knockdown.[28,29] The *miR-33* scaffold provides a valuable tool for achieving on-target, potent silencing that is deliverable via rAAVs or other viral vectors for research and clinical applications.

MATERIALS AND METHODS

Vector Design, Construction, and Production

To generate the rAAV constructs harboring sequences encoding endogenous miRNAs, pri-miRNA fragments were PCR amplified from mouse genomic DNA and cloned into the PpuMI site in the intronic region of pAAVsc-*CB-PI-Gluc* plasmid.[30] The identity of each pri-miRNA was verified by Sanger sequencing. shRNA fragments were generated by oligonucleotide annealing and cloned after the *U6* or *H1* promoter in pAAVsc-*CB-Egfp*.[16] The shRNA^{miR} fragments were incorporated into the intronic region of pAAVsc-*CB-PI-Gluc* or pAAVsc-*CB-Egfp*. An Excel macro was developed and can be used to design *shRNA*$^{miR\text{-}33}$ cassettes (Data S1). The RNAi sensor plasmids were made by incorporating a partial target coding sequence (CDS) after the β-galactosidase reporter gene in the pmiCHECK plasmid.[31] Table S1 shows the sequence of oligonucleotides for amplifying *mmu*-pri-miRNAs, generating shRNA fragments for gene silencing and partial CDS for constructing sensor plasmids. The shRNA$^{miR\text{-}33}$ was synthesized as gBlocks (IDT). AAV vectors used in this study were generated, purified, and titered as described previously.[32]

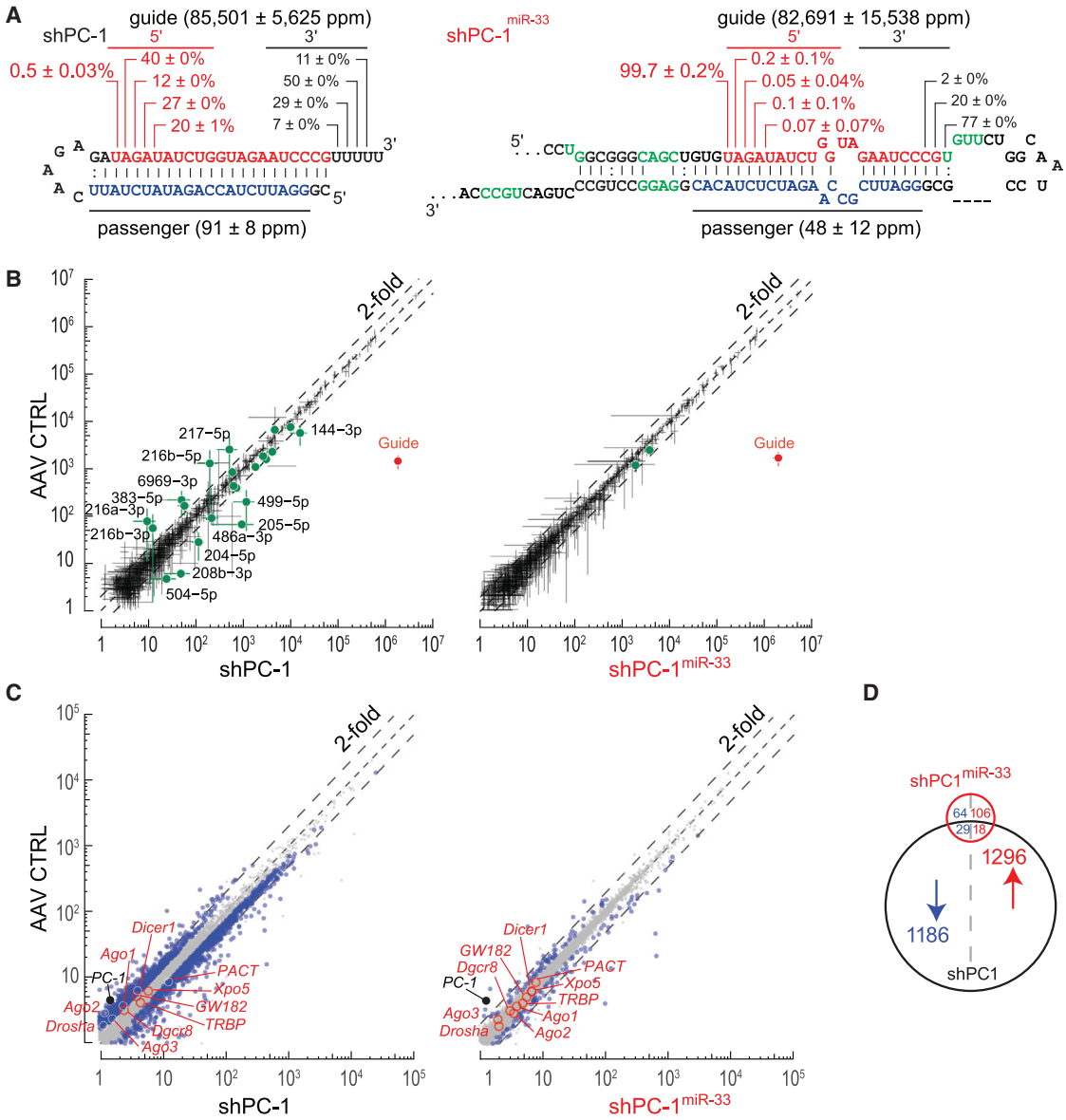

Figure 5. Small RNA and Transcriptome Analysis in Mouse Liver

Adult C57BL/6 mice were treated with 1.0×10^{11} GCs rAAV9-*shPC-1*, rAAV9-*shPC-1*$^{miR-33}$, or rAAV vector without shRNA by tail vein injection. After 3 weeks, mice were sacrificed, and liver RNA was extracted and used for the following small silencing RNA (A), endogenous miRNA (B), and global gene expression analyses (C). (A) Profiling of 5′ and 3′ distribution of guide (red) and passenger (blue) strands of silencing RNAs detected in mice by small RNA-seq (mean ± SD, n = 3). (B) Scatterplots comparing the abundance of endogenous miRNAs and small RNAs following treatment with AAV control (y axis) and AAV-*shPC-1* (x axis, left plot) or AAV-*shPC-1*$^{miR-33}$ (x axis, right plot). Each point represents the normalized miRNA reads in parts per million (ppm) averaged from three biological replicates. Error bar represents SD (n = 3). Differentially expressed miRNAs (adjusted $p < 0.05$) are in green solid dots. The guide strand is indicated in red. (C) Comparison of mRNA abundance in whole transcriptome analysis. Each point represents the mean fragments per kilobase of exon model per million reads mapped (FPKM) value of a single gene (n = 3). Significantly dysregulated mRNAs are represented in blue dots. Genes associated with the RNAi pathway are annotated with open red circles (no change) or red dots (significantly changed). *PC-1* is annotated with a solid black dot. (D) A Venn diagram summarizing differentially expressed genes in *shPC-1*$^{miR-33}$- and *shPC-1*-treated mice. GC, genome copy.

Cell Culture and Reporter Assay

HEK293 cells were cultured in DMEM supplemented with 10% FBS and 100 mg/L of penicillin-streptomycin (HyClone). Cells were maintained in a humidified incubator at 37°C and 5% CO_2. Plasmids were transfected into cells in 24-well plates using Lipofectamine 2000 (Invitrogen). After 48 h, cells were lysed, and 10 μL lysates was used for the β-galactosidase assay using the Galacto-Star System (Applied Biosystems), according to the manufacturer's instructions.

Firefly luciferase activity was assessed using the Luciferase Assay System (Promega) with the same amount of lysate for β-galactosidase assay in accordance with the manufacturer's instructions.

Southern Blot Analysis for Hirt DNA and Vector DNA Analysis

Low-molecular-weight Hirt DNA was extracted from triple plasmid-transfected HEK293 cells[33] and digested with DpnI before hybridization. The *Egfp* fragment was labeled by ^{32}P as probe using a random primer labeling kit (Takara). The blots were visualized using a FLA-7000 Imager (Fujifilm), and densitometry analyses were performed using MultiGauge software (Fujifilm). Viral DNAs were extracted from purified vectors following procedures for extraction of recombinant adenovirus genomic DNA.[16,32] Vector DNAs equivalent to 1×10^{10} to 1×10^{11} genomes were loaded onto agarose gels, stained with ethidium bromide, and analyzed with Image Lab software (Bio-Rad).

Small RNA Northern Blot Analysis

HEK293 cells in 10-cm cell culture dishes were transfected with *shRNA* or *shRNA$^{miR\text{-}33}$* plasmids using Lipofectamine 2000. After 48 h, total RNA was extracted using TRIzol (Invitrogen). Five micrograms of total RNA was used for small RNA northern blot analysis as described previously.[30] Synthetic DNA oligonucleotides were used as reference for quantification analyses or labeled with γ-^{32}P ATP using T4 polynucleotide kinase (NEB) as probes (Table S1).

Mouse Studies

Male C57BL/6 mice at 6–8 weeks old (Harlan, IN, USA) were sacrificed 3 weeks after intravenous injection of rAAV vectors at indicated doses. Bioluminescence levels were measured by IVIS-100 system, and liver tissues were harvested for downstream analysis. Firefly luciferase activities in mouse livers were assessed using the Luciferase Assay System (Promega) with 10 μg of liver protein. Total liver RNA was extracted using TRIzol (Invitrogen). qRT-PCR was performed as reported before.[30] Primers used in the study are shown in Table S1. All animal procedures were performed according to the guidelines of the Institutional Animal Care and Use Committee of University of Massachusetts Medical School.

Small RNA Library Construction and Analysis

Total liver RNA (40 μg) was purified by 15% urea polyacrylamide gel electrophoresis (PAGE), selecting for 18- to 30-nt-long RNAs. Ligation of the 3′ adaptor (5′-rApp TGG AAT TCT CGG GTG CCA AGG /ddC/-3′) was done using truncated, K227Q mutant T4 RNA Ligase 2 at 25°C for ≥16 h. 5′ Adaptor (5′-GUU CAG AGU UCU ACA GUC CGA CGA UC-3′) was added using T4 RNA ligase (Ambion) at 25°C for ≥2 h, followed by reverse transcription using avian myeloblastosis virus (AMV) reverse transcriptase and PCR using Q5 polymerase (NEB). An Illumina NextSeq550 was used for high-throughput, single-end 50-nt sequencing. The 3′ adaptors of small RNA libraries were removed using Flexbar 3.0.3.[34] After trimming, only reads with Phred scores at each position higher than 20 were kept for downstream analysis. Such reads were first aligned with Bowtie v.1.2.1.1[35] to miRNA hairpins[36] supplemented with corresponding hairpin backbones of *miR-33* and shRNA. Tailed reads were discovered with Tailor v.1.1.[37] Differential analysis was done with DESeq v.3.5.[38]

RNA Sequencing Analysis

Strand-specific RNA sequencing (RNA-seq) libraries were prepared as described previously.[39] Paired-end RNA-seq reads were first aligned to ribosomal RNA (BK000964.1) with Bowtie2.[40] Non-rRNA reads were subsequently used for gene quantification with Salmon v.0.8.2.[41] Differential analysis was performed using DESeq v.3.5.[38] Data processing and figures were prepared with R v.3.4.1.[42]

Statistical Analysis

All results are shown as mean ± SD and compared between groups using two-tailed Student's t test, except for Figure 1F data, which used Fisher's exact test.

Accession Numbers

The raw sequencing data reported here have been deposited to the NCBI Sequence Read Archive (SRA) under the accession number SRA: SRP124896.

SUPPLEMENTAL INFORMATION

Supplemental Information can be found online at https://doi.org/10.1016/j.ymthe.2019.11.018.

AUTHOR CONTRIBUTIONS

J.X., P.D.Z., and G.G. designed the experiments. J.X., S.G., S.Z., Y.W., C.L., C.C., Q.S., R.H., J.L., H.Y., and J.K. performed the experiments. C.L. from Fornax Biotech LLC led the analysis of high-throughput sequencing data. P.W.L.T. and R.H. assisted in high-throughput sequencing data analysis. A.B. wrote the Excel macro for the design of shRNA$^{miR\text{-}33}$. P.W.L.T. and A.B. helped with manuscript editing. J.X. and C.L. prepared the figures. J.X., P.D.Z., and G.G. wrote the manuscript.

CONFLICTS OF INTEREST

G.G. is a scientific co-founder of Aspa Therapeutics, Inc., holds equity in the company, and is an inventor on patents with potential royalties licensed to Aspa Therapeutics, Inc. G.G. and P.D.Z. are founders of Voyager Therapeutics, hold equity in the company, and are inventors on patents with potential royalties licensed to Voyager Therapeutics and other biopharmaceutical companies.

ACKNOWLEDGMENTS

G.G. is supported by grants from the University of Massachusetts Medical School (an internal grant) and the NIH (R01NS076991-01, 1P01AI100263-01, 4P01HL131471-02, and R01HL097088).

REFERENCES

1. Guo, H., Ingolia, N.T., Weissman, J.S., and Bartel, D.P. (2010). Mammalian microRNAs predominantly act to decrease target mRNA levels. Nature *466*, 835–840.

2. Elbashir, S.M., Harborth, J., Lendeckel, W., Yalcin, A., Weber, K., and Tuschl, T. (2001). Duplexes of 21-nucleotide RNAs mediate RNA interference in cultured mammalian cells. Nature *411*, 494–498.

3. Gao, G., Vandenberghe, L.H., and Wilson, J.M. (2005). New recombinant serotypes of AAV vectors. Curr. Gene Ther. *5*, 285–297.

4. Grimm, D., Streetz, K.L., Jopling, C.L., Storm, T.A., Pandey, K., Davis, C.R., Marion, P., Salazar, F., and Kay, M.A. (2006). Fatality in mice due to oversaturation of cellular microRNA/short hairpin RNA pathways. Nature *441*, 537–541.

5. McBride, J.L., Boudreau, R.L., Harper, S.Q., Staber, P.D., Monteys, A.M., Martins, I., Gilmore, B.L., Burstein, H., Peluso, R.W., Polisky, B., et al. (2008). Artificial miRNAs mitigate shRNA-mediated toxicity in the brain: implications for the therapeutic development of RNAi. Proc. Natl. Acad. Sci. USA *105*, 5868–5873.

6. Giering, J.C., Grimm, D., Storm, T.A., and Kay, M.A. (2008). Expression of shRNA from a tissue-specific pol II promoter is an effective and safe RNAi therapeutic. Mol. Ther. *16*, 1630–1636.

7. Pfister, E.L., Chase, K.O., Sun, H., Kennington, L.A., Conroy, F., Johnson, E., Miller, R., Borel, F., Aronin, N., and Mueller, C. (2017). Safe and Efficient Silencing with a Pol II, but Not a Pol lII, Promoter Expressing an Artificial miRNA Targeting Human Huntingtin. Mol. Ther. Nucleic Acids *7*, 324–334.

8. Boudreau, R.L., Martins, I., and Davidson, B.L. (2009). Artificial microRNAs as siRNA shuttles: improved safety as compared to shRNAs in vitro and in vivo. Mol. Ther. *17*, 169–175.

9. Fowler, D.K., Williams, C., Gerritsen, A.T., and Washbourne, P. (2016). Improved knockdown from artificial microRNAs in an enhanced miR-155 backbone: a designer's guide to potent multi-target RNAi. Nucleic Acids Res. *44*, e48.

10. Maepa, M.B., Ely, A., Grayson, W., and Arbuthnot, P. (2017). Sustained Inhibition of HBV Replication In Vivo after Systemic Injection of AAVs Encoding Artificial Antiviral Primary MicroRNAs. Mol. Ther. Nucleic Acids *7*, 190–199.

11. Boudreau, R.L., Monteys, A.M., and Davidson, B.L. (2008). Minimizing variables among hairpin-based RNAi vectors reveals the potency of shRNAs. RNA *14*, 1834–1844.

12. Jackson, A.L., and Linsley, P.S. (2010). Recognizing and avoiding siRNA off-target effects for target identification and therapeutic application. Nat. Rev. Drug Discov. *9*, 57–67.

13. Guda, S., Brendel, C., Renella, R., Du, P., Bauer, D.E., Canver, M.C., Grenier, J.K., Grimson, A.W., Kamran, S.C., Thornton, J., et al. (2015). miRNA-embedded shRNAs for Lineage-specific BCL11A Knockdown and Hemoglobin F Induction. Mol. Ther. *23*, 1465–1474.

14. Maczuga, P., Lubelski, J., van Logtenstein, R., Borel, F., Blits, B., Fakkert, E., Costessi, A., Butler, D., van Deventer, S., Petry, H., et al. (2013). Embedding siRNA sequences targeting apolipoprotein B100 in shRNA and miRNA scaffolds results in differential processing and in vivo efficacy. Mol. Ther. *21*, 217–227.

15. Gu, S., Jin, L., Zhang, Y., Huang, Y., Zhang, F., Valdmanis, P.N., and Kay, M.A. (2012). The loop position of shRNAs and pre-miRNAs is critical for the accuracy of dicer processing in vivo. Cell *151*, 900–911.

16. Xie, J., Mao, Q., Tai, P.W.L., He, R., Ai, J., Su, Q., Zhu, Y., Ma, H., Li, J., Gong, S., et al. (2017). Short DNA Hairpins Compromise Recombinant Adeno-Associated Virus Genome Homogeneity. Mol. Ther. *25*, 1363–1374.

17. Auyeung, V.C., Ulitsky, I., McGeary, S.E., and Bartel, D.P. (2013). Beyond secondary structure: primary-sequence determinants license pri-miRNA hairpins for processing. Cell *152*, 844–858.

18. Fang, W., and Bartel, D.P. (2015). The Menu of Features that Define Primary MicroRNAs and Enable De Novo Design of MicroRNA Genes. Mol. Cell *60*, 131–145.

19. Fellmann, C., Hoffmann, T., Sridhar, V., Hopfgartner, B., Muhar, M., Roth, M., Lai, D.Y., Barbosa, I.A., Kwon, J.S., Guan, Y., et al. (2013). An optimized microRNA backbone for effective single-copy RNAi. Cell Rep. *5*, 1704–1713.

20. Chourabi, M., Liew, M.S., Lim, S., H'mida-Ben Brahim, D., Boussofara, L., Dai, L., Wong, P.M., Foo, J.N., Sriha, B., Robinson, K.S., et al. (2018). ENPP1 Mutation Causes Recessive Cole Disease by Altering Melanogenesis. J. Invest. Dermatol. *138*, 291–300.

21. Davidson, B.L., and McCray, P.B., Jr. (2011). Current prospects for RNA interference-based therapies. Nat. Rev. Genet. *12*, 329–340.

22. Borel, F., Gernoux, G., Sun, H., Stock, R., Blackwood, M., Brown, R.H., Jr., and Mueller, C. (2018). Safe and effective superoxide dismutase 1 silencing using artificial microRNA in macaques. Sci. Transl. Med. *10*, eaau6414.

23. Boudreau, R.L., Spengler, R.M., and Davidson, B.L. (2011). Rational design of therapeutic siRNAs: minimizing off-targeting potential to improve the safety of RNAi therapy for Huntington's disease. Mol. Ther. *19*, 2169–2177.

24. Ding, H., Liao, G., Wang, H., and Zhou, Y. (2007). Asymmetrically designed siRNAs and shRNAs enhance the strand specificity and efficacy in RNAi. J. RNAi Gene Silencing *4*, 269–280.

25. Mockenhaupt, S., Grosse, S., Rupp, D., Bartenschlager, R., and Grimm, D. (2015). Alleviation of off-target effects from vector-encoded shRNAs via codelivered RNA decoys. Proc. Natl. Acad. Sci. USA *112*, E4007–E4016.

26. Gu, S., Jin, L., Zhang, F., Huang, Y., Grimm, D., Rossi, J.J., and Kay, M.A. (2011). Thermodynamic stability of small hairpin RNAs highly influences the loading process of different mammalian Argonautes. Proc. Natl. Acad. Sci. USA *108*, 9208–9213.

27. Park, J.H., and Shin, C. (2015). Slicer-independent mechanism drives small-RNA strand separation during human RISC assembly. Nucleic Acids Res. *43*, 9418–9433.

28. Yang, Y.S., Xie, J., Wang, D., Kim, J.M., Tai, P.W.L., Gravallese, E., Gao, G., and Shim, J.H. (2019). Bone-targeting AAV-mediated silencing of Schnurri-3 prevents bone loss in osteoporosis. Nat. Commun. *10*, 2958.

29. Sweeney, C.G., Kearney, P.J., Fagan, R.R., Smith, L.A., Bolden, N.C., Zhao-Shea, R., Rivera, I.V., Kolpakova, J., Xie, J., Gao, G., et al. (2019). Conditional, inducible gene silencing in dopamine neurons reveals a sex-specific role for Rit2 GTPase in acute cocaine response and striatal function. Neuropsychopharmacology. Published online July 5, 2019. https://doi.org/10.1038/s41386-019-0457-x.

30. Xie, J., Ameres, S.L., Friedline, R., Hung, J.H., Zhang, Y., Xie, Q., Zhong, L., Su, Q., He, R., Li, M., et al. (2012). Long-term, efficient inhibition of microRNA function in mice using rAAV vectors. Nat. Methods *9*, 403–409.

31. He, X., Xie, J., Zhang, D., Su, Q., Sai, X., Bai, R., Chen, C., Luo, X., Gao, G., and Pan, W. (2015). Recombinant adeno-associated virus-mediated inhibition of microRNA-21 protects mice against the lethal schistosome infection by repressing both IL-13 and transforming growth factor beta 1 pathways. Hepatology *61*, 2008–2017.

32. Gao, G., and Sena-Esteves, M. (2012). Introducing genes into mammalian cells: viral vectors. In Molecular Cloning: A Laboratory Manual, *Volume 2*, M.R. Green and J. Sambrook, eds. (Cold Spring Harbor Laboratory Press), pp. 1209–1313.

33. Wang, X.S., Ponnazhagan, S., and Srivastava, A. (1995). Rescue and replication signals of the adeno-associated virus 2 genome. J. Mol. Biol. *250*, 573–580.

34. Roehr, J.T., Dieterich, C., and Reinert, K. (2017). Flexbar 3.0—SIMD and multicore parallelization. Bioinformatics *33*, 2941–2942.

35. Langmead, B., Trapnell, C., Pop, M., and Salzberg, S.L. (2009). Ultrafast and memory-efficient alignment of short DNA sequences to the human genome. Genome Biol. *10*, R25.

36. Kozomara, A., and Griffiths-Jones, S. (2014). miRBase: annotating high confidence microRNAs using deep sequencing data. Nucleic Acids Res. *42*, D68–D73.

37. Chou, M.T., Han, B.W., Hsiao, C.P., Zamore, P.D., Weng, Z., and Hung, J.H. (2015). Tailor: a computational framework for detecting non-templated tailing of small silencing RNAs. Nucleic Acids Res. *43*, e109.

38. Anders, S., and Huber, W. (2010). Differential expression analysis for sequence count data. Genome Biol. *11*, R106.

39. Zhang, Z., Theurkauf, W.E., Weng, Z., and Zamore, P.D. (2012). Strand-specific libraries for high throughput RNA sequencing (RNA-Seq) prepared without poly(A) selection. Silence *3*, 9.

40. Langmead, B., and Salzberg, S.L. (2012). Fast gapped-read alignment with Bowtie 2. Nat. Methods *9*, 357–359.

41. Patro, R., Duggal, G., Love, M.I., Irizarry, R.A., and Kingsford, C. (2017). Salmon provides fast and bias-aware quantification of transcript expression. Nat. Methods *14*, 417–419.

42. R Development Core Team. (2017). R: A language and environment for statistical computing (R Foundation for Statistical Computing).

YMTHE, Volume *28*

Supplemental Information

Effective and Accurate Gene Silencing by a Recombinant AAV-Compatible MicroRNA Scaffold

Jun Xie, Phillip W.L. Tai, Alexander Brown, Shoufang Gong, Sha Zhu, Yi Wang, Chengjian Li, Cansu Colpan, Qin Su, Ran He, Hong Ma, Jia Li, Hanqing Ye, Jihye Ko, Phillip D. Zamore, and Guangping Gao

Supplementary Figure 1

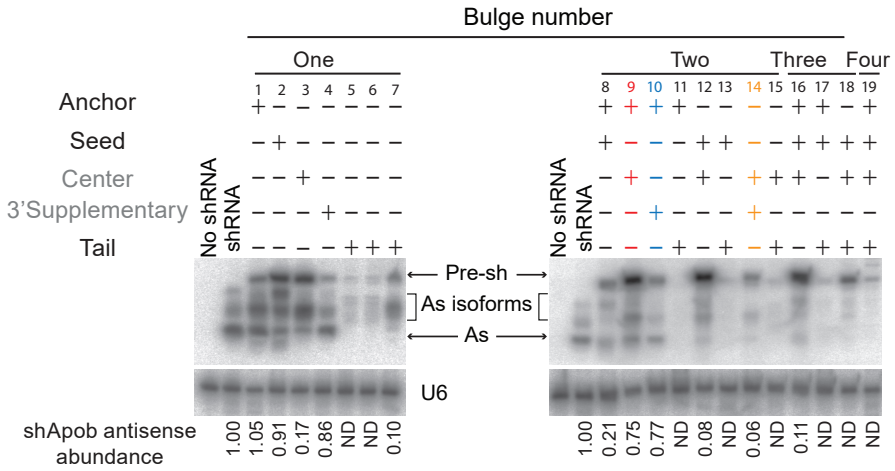

Supplementary Figure 1. Small RNA Northern blot analysis of shApob antisense levels in HEK293 cells transfected with the shApob constructs with/without bulge. As, shApob antisense; Pre-sh, shApob precursors.

Supplementary Figure 2

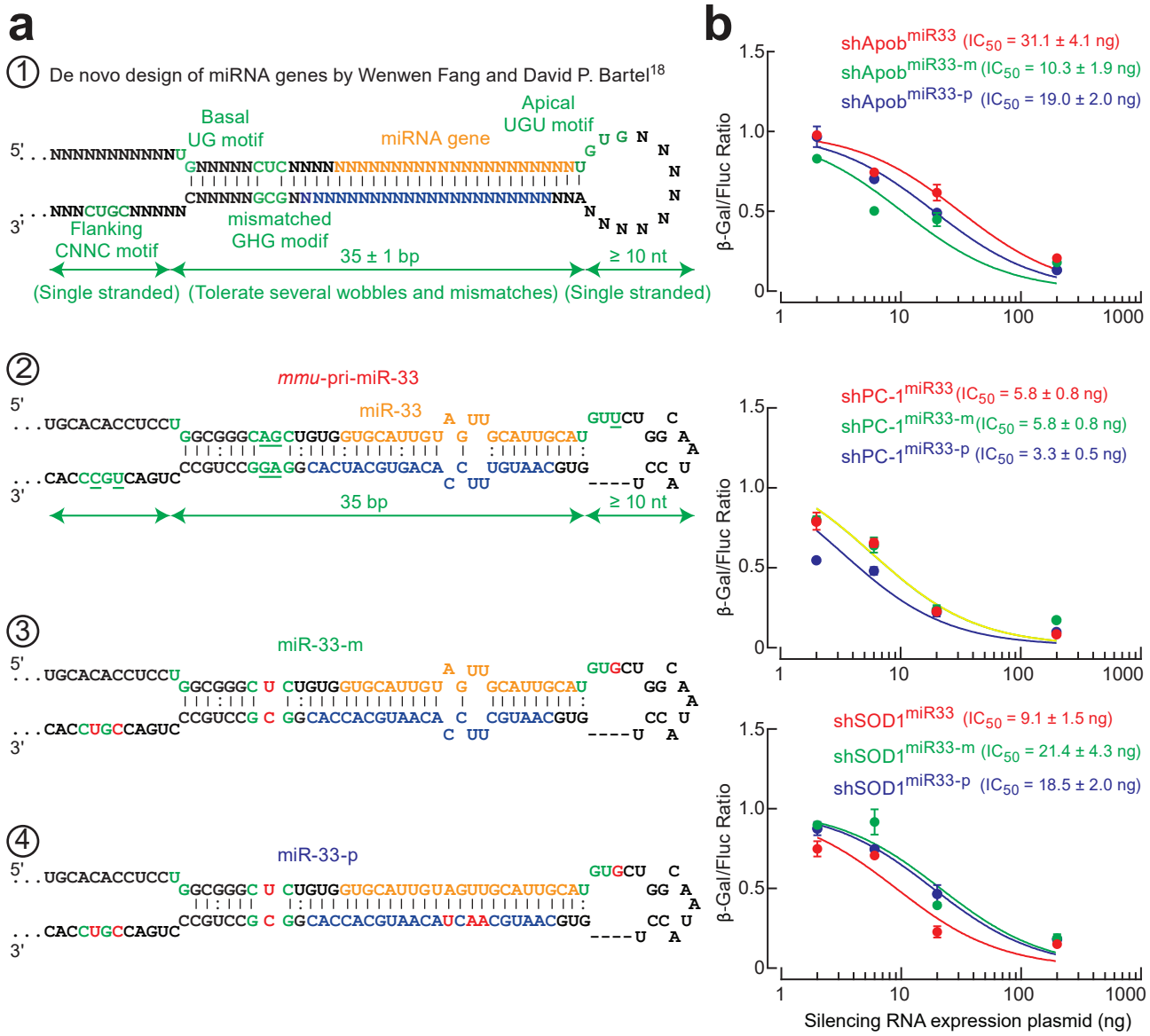

Supplementary Figure 2. Engineering the motif features of miRNA genes into the pri-mmu-miR-33 scaffold.

(a) Motifs (nucleotides in green) in miRNA genes described by Weiwei Fu and David P Bartel[29] (structure 1) and in *mmu*-pri-miR-33 (structure 2). The underlined variable nucleotides in *mmu*-pri-miR-33 were converted into the motifs of miRNA genes (red nucleotides in structures 3 and 4) to generate two modified miR-33 scaffolds. (b) Dose response curves for knockdown efficacy in the *Apob*, *PC1*, and SOD1 genes in HEK293 cells transfected with the shRNA$^{miR\text{-}33}$ and modified shRNA$^{miR\text{-}33}$ plasmids from 2 to 200 ng/well, together with their sensor plasmids (200 ng/well). Values are mean ± SD. IC50 values are listed for each construct. Note that the shPC-1$^{miR\text{-}33}$ and shPC-1$^{miR33\text{-}m}$ datapoints are overlapping (yellow curve).

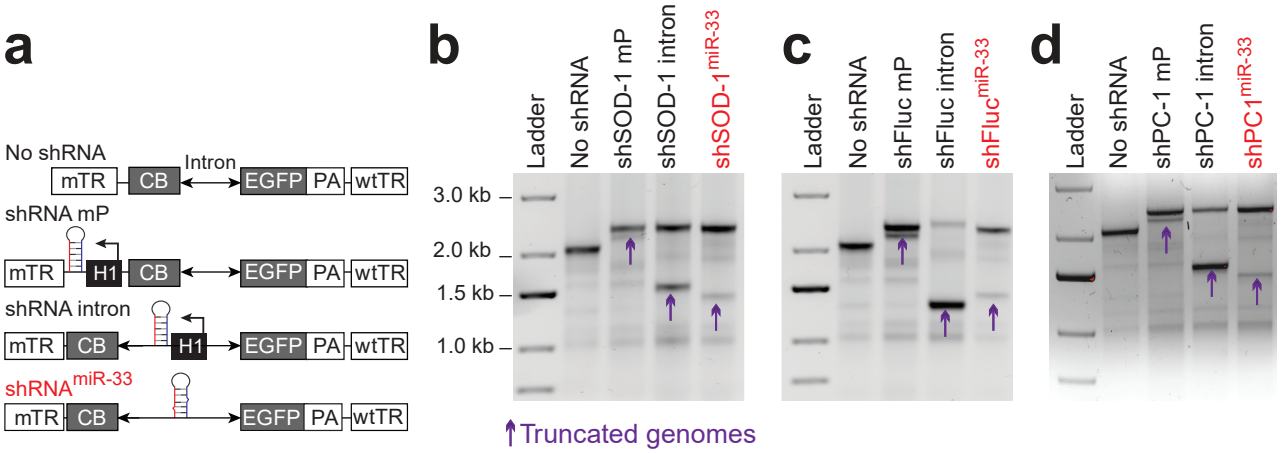

Supplementary Figure 3. Vector genome populations in purified rAAV gene silencing vectors

(a) Schematic of gene silencing constructs used for AAV packaging. (b-d) Agarose gel analysis of viral DNA extracted from purified vectors harboring shRNA or shRNA^{miR-33} against SOD-1, Fluc, and *PC*-1. The shFluc intron vector in panel (c) harbors the shRNA cassette in close proximity to the EGFP transgene, while the intronic shSOD-1 and shPC-1 vectors harbor the shRNA cassette in close proximity to the CB promoter as shown in panel (a). Purple arrows indicate truncated genomes caused by shRNA-encoding sequences or the miR-33 scaffold. The small truncated genomes are caused by obligate palindromic sequences residing in vector genomes as we previously reported[16].

Supplementary Figure 4

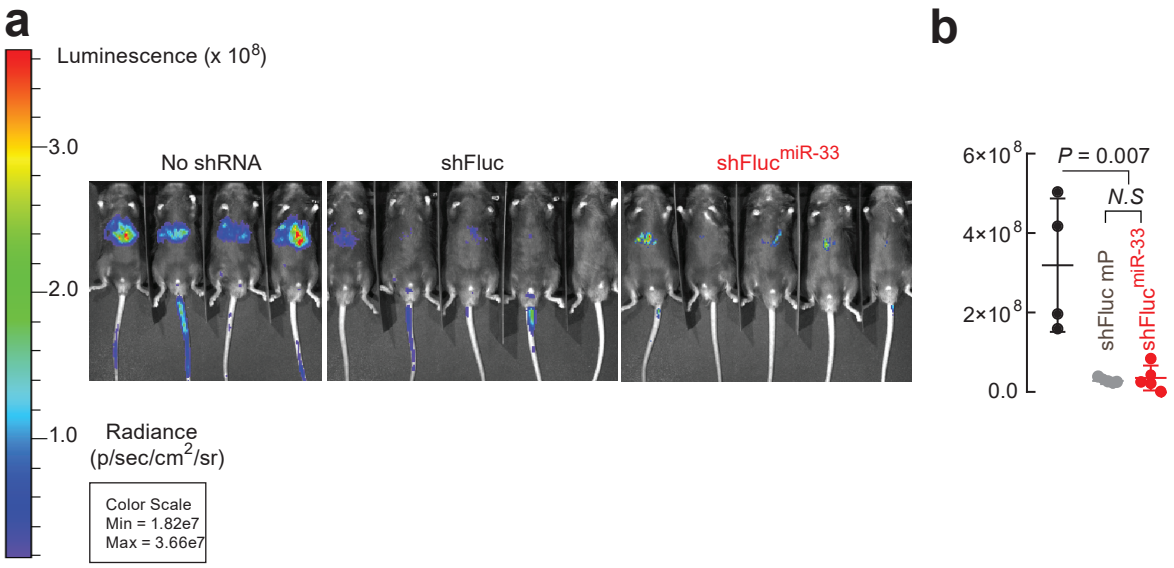

Supplementary Figure 4. Bioluminescence levels from mice co-injected with rAAV9-Fluc at 1.0 × 10^{11} GCs/mouse and rAAV9-no shRNA , shFluc, or shFluc^{miR-33} at 5.0 × 10^{11} GCs/mouse. (a) Live luminescence maging of mice treated with AAV vectors for three weeks. (b) Photo flux of liver region.

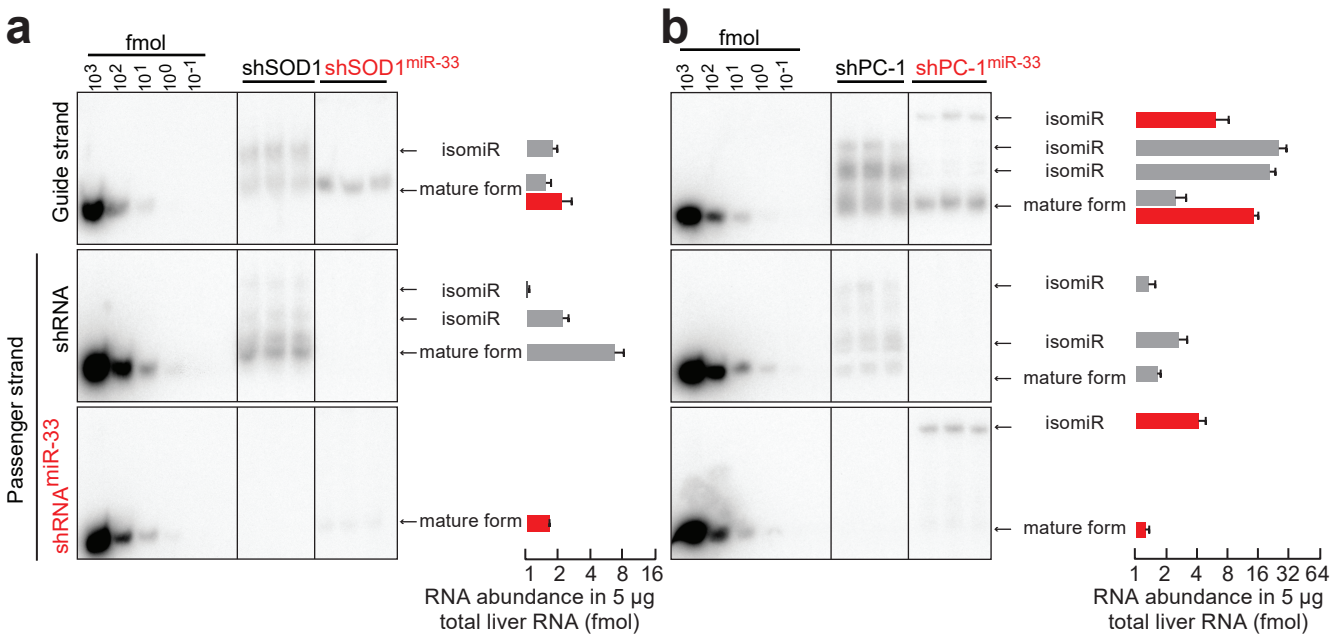

Supplementary Figure 5. Northern blot analysis of transcribed RNA from shSOD1 or shSOD1^{miR-33} (a), shPC-1 or shPC-1^{miR-33} (b) in HEK 293 cells.

Total RNA was extracted from the HEK 293 cells 48 hours after transfection. Five micrograms of total RNA were used for Northern blot analysis. Synthetic oligonucleotides at indicated amount were used as reference for quantification. The transcribed RNAs from shRNA and shRNA^{miR-33} are in grey and red, respectively.

Supplementary Figure 6

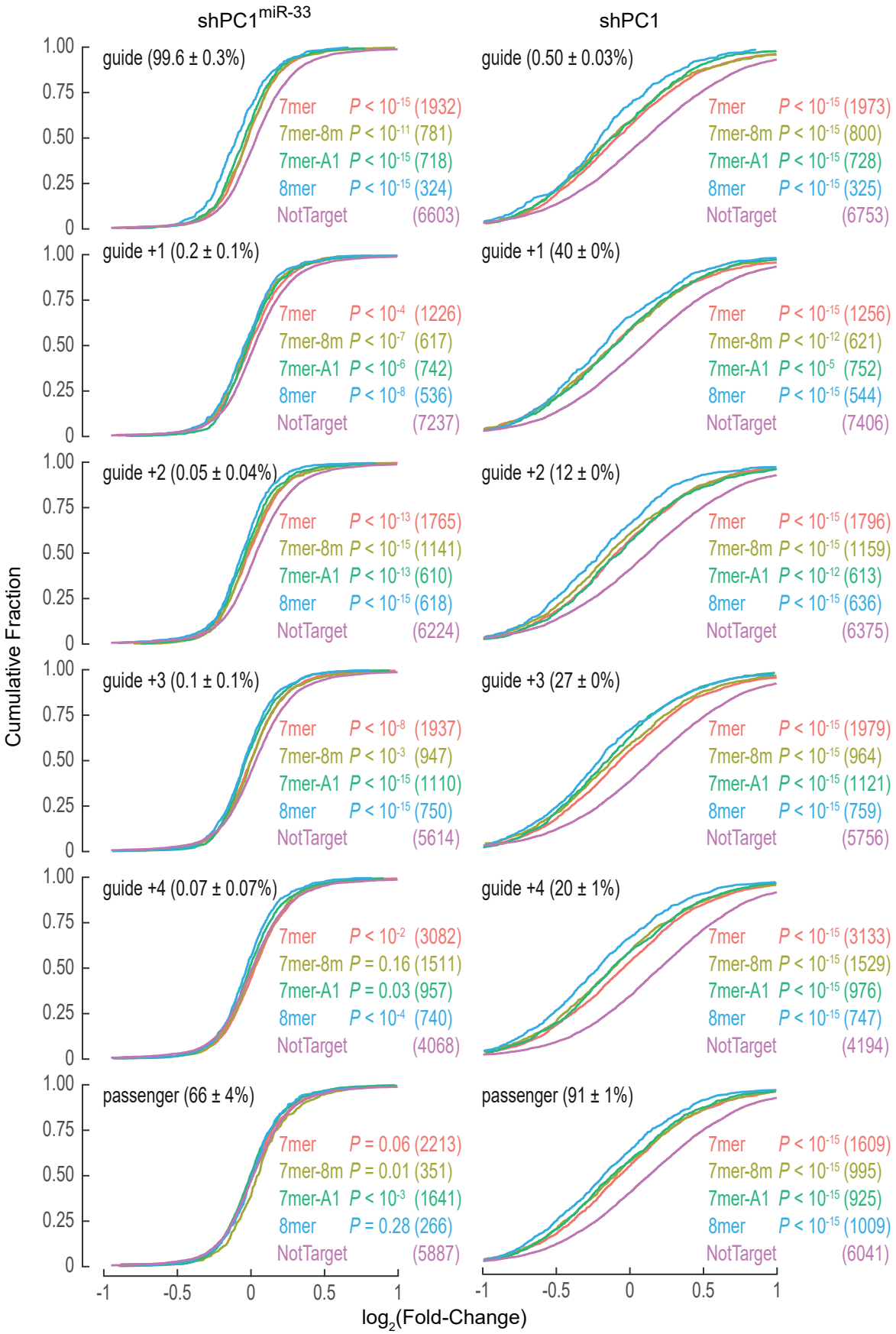

Supplementary Figure 6. Imprecise process of shRNA causes off-target knockdown.

Protein-coding genes are categorized based on pairing of their 3' UTR sequences to difference guide isoforms. The acumulative distribution of log $_2$ fold-change compared to control (NotTarget) is plotted. Guide +1, +2, +3, or +4: guide isoform whose 5' ends shift 1, 2, 3, or 4 nucleotides towards the 3' end.

Supplementary Table 1: Oligonucleotides used in this study.

Oligonucleotides	Sequence (5′ to 3′)	Aims
pri-miR-122 F	ATCGGGCCCGACTGCAGTTTCAGCGTTTG	Cloning of mouse *pri-miR-122*
pri-miR-122 R	CGCGGGCCCGACTTTACATTACACACAAT	
pri-miR-33 F	AGGGCTCTGCGTTTGCTCCAGG	Cloning of mouse *pri-miR-33*
pri-miR-33 R	AGGGTGACACTGTCCTTATT	
pri-miR-26a F	GCCCCTTCTCTTTGGCAG	Cloning of mouse *pri-miR-26a*
pri-miR-26a R	TTGGCCAGCAAGCTTGG	
pri-miR-126 F	GGAAGGCATTGTGGGGCGTAA	Cloning of mouse *pri-miR-126*
pri-miR-126 R	TGCAAAGTCTCTGGCTGTC	
pri-miR-22 F	ATTTCAGGTCGTCCCATATGTC	Cloning of mouse *pri-miR-22*
pri-miR-22 R	GTCCCTCACCTTCCGGATGATAG	
pri-miR-199 F	CTCAGTCCTGGGCCTACTTTTTCCA	Cloning of mouse *pri-miR-199*
pri-miR-199 R	TGCCACGTCAGAAGAGTTCAG	
pri-miR-99 F	GGATTCCCAGCCTTTAAAATATTTAC	Cloning of mouse *pri-miR-99*
pri-miR-99 R	GGATTAAAAGATCCATGAAG	
pri-miR-21 F	GATATCGACTGTTGGCATTAAGCCCC	Cloning of mouse *pri-miR-21*
pri-miR-21 R	GACTTTCCAAGTCTCACAAG	
pri-miR-375 F	ACCGCGGTGCTCAGGTGAGAG	Cloning of mouse *pri-miR-375*
pri-miR-375 R	CAGAGACTGAGCACGGT	
pri-miR-101 F	TTTTGCCTCCATCCAGAAGTGC	Cloning of mouse *pri-miR-101*
pri-miR-101 R	GGAAGAGTGGTGAACACAGGA	
pri-miR-451 F	AGTCTGGGTACCCCACCTCCAGAG	Cloning of mouse *pri-miR-451*
pri-miR-451 R	GCACAGTGAAGAGGAAAATGTACCC	
pri-miR-194 F	AGGTACAGGCTAGGTCTTGTCC	Cloning of mouse *pri-miR-194*
pri-miR-194 R	AGCTCCGTGCTCCGTAGTCT	
pri-miR-30a F	GTGTTTGACACTTAGTAGATGA	Cloning of mouse *pri-miR-30a*
pri-miR-30a R	AATATATTTCTTTGCTTAGC	
pri-miR-155 F	TTTCTCTTTGCAGGTGCTGC	Cloning of mouse *pri-miR-155*

pri-miR-155 R	GTCTGACATCTACGTTCATC	
shApob	CTGACTTTCATCTGTACTACATTCAAGAGATGTAGTACAG ATGAAAGTCAGTTTTT	Synthetic oligo for silencing *Apob* gene
shPC1	CGGGATTCTACCAGATATCTATTCAAGAGATAGATATCTG GTAGAATCCCGTTTTT	Synthetic oligo for silencing *PC1* gene
shSOD1	CATCATCAATTTCGAGCAGAATTCAAGAGATTCTGCTCGA AATTGATGATGTTTTT	Synthetic oligo for silencing SOD1 gene
shFluc	TTGACAAATACGATTTATCTATTCAAGAGATAGATAAATC GTATTTGTCAATTTTT	Synthetic oligo for silencing *Fluc* gene
Apob sensor-F	CGCCTCGAGAAATTGAAGAAGATCTGTTAAC	To generate partial *Apob* CDS as shApob sensor element
Apob sensor-R	CGCGCGGCCGCTCTTCTCTGGAGGGGACTGT	
PC1 sensor-F	CGCCTCGAGCCCAAAATGAATGCTTCTTTCTCG	To generate partial *PC1* CDS as shPC1 sensor element
PC1 sensor-R	CGCGCGGCCGCCCTGAAGAATCTGGTTCTTC	
hSOD1 sensor-F	ATAACTCGAGCGAAGGCCGTGTGCGTGCTGAAGGGC	To generate partial *hSOD1* CDS as shSOD1 sensor element
hSOD1 sensor-R	GCCAGCGGCCGCTTGGGCGATCCCAATTACACCACAAG	
shApob^{miR-33} gBlock	AGATCTAGGGCTCTGCGTTTGCTCCAGGTAGTCCGCTGCT CCCTTGGGCCTGGGCCCACTGACAGCCCTGGTGCCTCTGG CCGGCTGCACACCTCCTGGCGGGCAGCTGTGTGTAGTAC AGATGAAAGTCAGTGTTCTGGCAATACCTGCTGACTTTAC TATGTACTACACACGGAGGCCTGCCCTGACTGCCCACGGT GCCGTGGCCAAAGAGGATCTAAGGGCACCGCTGAGGGCC TACCTAACCATCGTGGGGAATAAGGACAGTGTCACCCTTT TTCTGCAG	To generate *shApob^{miR-33}*
shPC1^{miR-33} gBlock	AGATCTAGGGCTCTGCGTTTGCTCCAGGTAGTCCGCTGCT CCCTTGGGCCTGGGCCCACTGACAGCCCTGGTGCCTCTGG CCGGCTGCACACCTCCTGGCGGGCAGCTGTGTAGATATCT GGTAGAATCCCGTGTTCTGGCAATACCTGCGGGATTCGCC AAGATCTCTACACGGAGGCCTGCCCTGACTGCCCACGGT GCCGTGGCCAAAGAGGATCTAAGGGCACCGCTGAGGGCC TACCTAACCATCGTGGGGAATAAGGACAGTGTCACCCTTT TTCTGCAG	To generate *shPC1^{miR-33}*
shSOD1^{miR-33} gBlock	AGATCTAGGGCTCTGCGTTTGCTCCAGGTAGTCCGCTGCT CCCTTGGGCCTGGGCCCACTGACAGCCCTGGTGCCTCTGG CCGGCTGCACACCTCCTGGCGGGCAGCTGTGTTCTGCTCG AAATTGATGATGTGTTCTGGCAATACCTGCATCATCATAT CCGAGCAGAACACGGAGGCCTGCCCTGACTGCCCACGGT GCCGTGGCCAAAGAGGATCTAAGGGCACCGCTGAGGGCC TACCTAACCATCGTGGGGAATAAGGACAGTGTCACCCTTT TTCTGCAG	To generate *shSOD1^{miR-33}*
shFluc^{miR-33} gBlock	AGATCTAGGGCTCTGCGTTTGCTCCAGGTAGTCCGCTGCT CCCTTGGGCCTGGGCCCACTGACAGCCCTGGTGCCTCTGG CCGGCTGCACACCTCCTGGCGGGCAGCTGTGTAGATAAA TCGTATTTGTCAATGTTCTGGCAATACCTGTTGACAAAAT CAATTTATCTACACGGAGGCCTGCCCTGACTGCCCACGGT GCCGTGGCCAAAGAGGATCTAAGGGCACCGCTGAGGGCC TACCTAACCATCGTGGGGAATAAGGACAGTGTCACCCTTT TTCTGCAG	To generate *shFluc^{miR-33}*
Apob-F	GTCCAGGTTGAATCACGGGT	qRT-PCR for *apob* mRNA
Apob-R	AGGATCCTGCAAGGTCAAGC	

PC1-F	AAAGGCCGCTGCTTTGAAAG	qRT-PCR for *pc1* mRNA
PC1-R	CCGCACCTGAATTTGTTGCA	
Actin-F	ATGCCAACACAGTGCTGTCTGG	qRT-PCR for *actin* mRNA
Actin-R	TGCTTGCTGATCCACATCTGCT	
Egfp-F	AGCAAAGACCCCAACGAGAA	Quantification of AAV genome copies in liver and AAV vector preparations
Egfp-R	GGCGGCGGTCACGAA	
Egfp-probe	6FAM-CGCGATCACATGGTCCTGCTGG-TAMRA	
shApob and shApob^{miR-33} AS probe; standard for *shApob sense*	GACTTTCATCTGTACTACA	Probe and standard for small RNA Northern blot
shPC-1 and shPC-1^{miR-33} AS probe; standard for *shPC-1 sense*	CGGGATTCTACCAGATATCTA	
shSOD-1 and shSOD-1^{miR-33} AS probe; standard for *shSOD-1 sense*	CATCATCAATTTCGAGCAGAA	
shApob^{miR-33} sense probe	GTGTGTAGTACATAGTAAAGTC	
shPC-1^{miR-33} sense probe	GTGTAGATATCTTGGCGAATCC	
shSOD-1^{miR-33} sense probe	GTGTTCTGCTCGGATATGATGA	
shApob^{miR-33} sense reference	GACTTTACTATGTACTACACAC	
shPC-1^{miR-33} sense reference	GGATTCGCCAAGATATCTACAC	
shSOD-1^{miR-33} sense reference	TCATCATATCCGAGCAGAACAC	
shApob sense probe; standard for *shApob and shApob^{miR-33} AS*	TGTAGTACAGATGAAAGTCAG	
shPC-1 sense probe; standard for *shPC-1 and shPC-1^{miR-33} AS*	TAGATATCTGGTAGAATCCCG	
shSOD-1 sense probe; standard for *shSOD-1 and shSOD-1^{miR-33} AS*	TTCTGCTCGAAATTGATGATG	
U6 probe	CTCTGTATCGTTCCAATTTTAGTATA	

Supplementary Table 2: Decreased mRNAs in AAV-*shPC1* treated mice

Seed type	Guide	Guide+1	Guide+2	Guide+3	Guide+4
7mer	283	204	250	269	413
7mer-8m	131	107	192	163	241
7mer-A1	124	122	82	175	146
8mer	62	103	134	164	181
No Target	615	679	557	444	234
Sum	1215	1215	1215	1215	1215

Supplementary Table 3: Decreased mRNAs in AAV-*shPC1*$^{miR\text{-}33}$-treated mice

Seed type	Guide	Guide+1	Guide+2	Guide+3
7mer	18	15	17	16
7mer-8m	10	6	7	12
7mer-A1	8	3	6	3
8mer	6	9	13	8
Not Target	51	60	50	54
Sum	93	93	93	93

Supplementary Table 4: Dysregulated genes in AAV-*shPC1*$^{miR\text{-}33}$-treated mice and PC-1 loss-of-function patients

	Increased genes			Decreased genes	
	PC-1 loss-of-function patients vs healthy controls (fold)	AAV-*shPC1*$^{miR\text{-}33}$ vs AAV-*Egfp* treated mice (fold)		PC-1 loss-of-function patients vs healthy controls (fold)	AAV-*shPC1*$^{miR\text{-}33}$ vs AAV-*Egfp* treated mice (fold)
Ak1	5.4	2.7	*Arid5b*	0.11	0.71
Anp32b	11.3	2.4	*Fasn*	0.07	0.58
Hist1h1c	29.3	1.5	*Hmgcr*	< 0.01	0.59
Lrrc42	9	1.7	*Lss*	< 0.01	0.70
Map7d1	3.1	1.5	*Mme*	0.03	0.64
Mgat4b	7.4	1.6	*Tfrc*	0.23	0.66
Pgp	19.3	1.8	*Cers6*	0.03	0.68
Arhgef1	8.1	1.6	*Myc*	0.19	0.53
Col1a1	54.8	1.7	*Nt5e*	0.04	0.55
Gigyf1	2.7	1.6			
Ncor2	4.7	1.8			
Wdfy1	3.4	1.8			